ACS APPLIED MATERIALS & INTERFACES

Research Article

www.acsami.org

Temporary Single-Cell Coating for Bioprocessing with a Cationic Polymer

Ricardo D. C. Ribeiro,[†,‡] Deepali Pal,[§] David Jamieson,[∥] Kenneth S. Rankin,[‡,∥] Matthew Benning,[†] Kenneth W. Dalgarno,[†] and Ana M. Ferreira*[,†]

[†]School of Mechanical and Systems Engineering, Newcastle University, Newcastle Upon Tyne NE1 7RU, U.K.

[‡]Institute of Cellular Medicine, [§]Wolfson Childhood Cancer Research Centre, Northern Institute for Cancer Research, and [∥]Northern Institute for Cancer Research, Newcastle University, Newcastle Upon Tyne, NE2 4HH, U.K.

Supporting Information

ABSTRACT: Temporary single-cell coating is a useful tool for cell processing, allowing manipulation of cells to prevent cell attachment and agglomeration, before re-establishing normal cell function. In this work, a speckled coating method using a known polycation [poly(L-lysine), PLL] is described to induce cell surface electrostatic charges on three different cell types, namely, two bone cancer cell lines and fibroblasts. The morphology of the PLL speckled coating on the cell surface, internalization and metabolization of the polymer, and prevention of cellular aggregations are reported. Polymer concentration was found to be the key parameter controlling both capsule morphology and cell health. This approach allows a temporary cell coating over the course of 1−2 h, with cells exhibiting phenotypically normal behavior after ingesting and metabolizing the polymer. The process offers a fast and efficient alternative to aid single-cell manipulation for bioprocessing applications. Preliminary work on the application of PLL speckled cell coating in enabling reliable bioprinting is also presented.

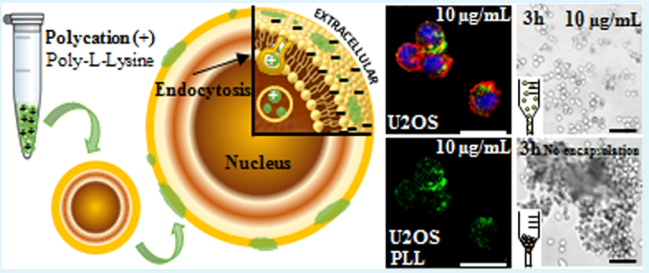

KEYWORDS: *coating, polycation, single cells, bioprocessing, cellular uptake, temporary, bioprinting*

1. INTRODUCTION

Cellular bioprocessing, cell-based sensors and devices, and cellular therapies require the positioning of cells within an instrument or the colocalization of different types of cells within a designed structure.[1] These techniques and systems normally rely on the preparation of cellular suspensions for further microprocessing. However, cells can end up aggregating and forming agglomerates measuring hundreds of micrometers in size. The lack of consistency in terms of conglomerate size and tendency to attach can significantly affect the reliability of processes, such as inkjet bioprinting.[2,3] Techniques to temporarily inhibit cell attachment to surfaces and particles and minimize cell agglomeration while cells are being manipulated would offer a valuable solution to this problem.

The encapsulation of isolated cells with artificial shells has been achieved through covalent surface modification or noncovalent adsorption of macromolecules onto the cell surface to introduce chemical functionalities into living cells.[4,5] Noncovalent cell surface modification offers the advantage over covalent techniques of minimal perturbation of the cell physiology, thereby preventing interference with important cellular functions governed by cell surface molecules.[4,6,7] Noncovalent surface modification has been achieved through layer-by-layer (LbL) methods with multiple layers of negatively and positively charged materials deposited on the material or cell surface.[8,9] This technique successfully avoids membrane disruption caused by electrostatic coating[10−14] a consequence of the lack of polysaccharides on mammal cell membrane.[9,15] This method also presents a number of tunable properties (layer number and composition, among others)[16] that allow it to be used effectively in different applications, including drug delivery.[17,18] However, it can be a laborious and time-consuming process,[19,20] as it requires multiple 10−15-min sequential depositions of oppositely charged monolayers onto the cell surface with intermediate washes,[21,22] with up to a 2-h interval between layers to guarantee good viability[11] and typically four to six bilayers.[9,23] To address these issues, the aim of this work was to develop a coating system with a cationic polymer to create electrostatic charges on the cell surface to aid single-cell manipulation by avoiding cellular agglomeration.

We describe a method to engineer single-cell surfaces based on the electrostatic adsorption of poly(L-lysine) (PLL) onto the cellular membrane. The coating morphology, internalization, and metabolization of PLL, as well as its effect on cell aggregation, are discussed. For fibroblasts and Ewing's sarcoma and osteosarcoma cells, cell health was found to be dependent on PLL concentration, with viabilities highest at the lowest concentration of PLL. Multiple internalization pathways are

Received: December 21, 2016
Accepted: March 21, 2017
Published: March 21, 2017

involved in the ingestion process, with cells exhibiting phenotypically normal behavior after metabolizing the polymer. The reported method is an effective way to avoid oversized cell conglomerates, demonstrated through simple agglomeration studies and high levels of repeatability in inkjet cell printing.

2. MATERIALS AND METHODS

2.1. Cell Culture. U2OS (ATTC; HTB-96), TC-71 (kindly donated by Dr. Britta Vormoor,[24] Newcastle University), and Neo-NHDF (Lonza) cells were cultured in high-glucose Dulbecco's Modified Eagle's Medium (DMEM; Life Technologies) supplemented with 10% fetal bovine serum (FBS; Sigma Life Science) and 5000 U/mL penicillin/streptomycin (Sigma Life Science) at 37 °C and 5% CO_2. All cell lines used in this study were obtained from the indicated suppliers and were tested for mycoplasma contamination.

2.2. Single-Cell Coating Method. Prior to the cell coating process, poly(L-lysine) hydrobromide (MW = 15−30 kDa, Sigma Life Science) was dialyzed for 2 days and then dissolved in Dulbecco's phosphate-buffered saline (DPBS; Sigma Life Science) until a concentration of 1 mg/mL had been reached. A 1 mg/mL solution of fluorescein isothiocyanate- (FITC-) labeled PLL (MW = 15−30 kDa, Sigma Life Science) was also prepared using DPBS. Both polymeric solutions were dissolved in Hanks' Balanced Salt Solution (HBSS) without phenol red (Sigma Life Science) at four different concentrations: 100, 50, 10, and 0 μg/mL (control). A cell suspension of 2×10^6 per 200 μL was prepared for each polymer concentration, and a volume of 1 mL was made up with HBSS without phenol red. The cells were incubated within the polymer for 15 min at 37 °C and 5% CO_2 for coating. Afterward, coated cells were washed twice with HBSS without phenol red, using centrifugation at 250*g* for 5 min to remove any polyelectrolyte excess.

2.3. Cytotoxicity Assays. Caspase-3 activity detection and membrane permeability assay was adapted from the manufacturer instructions (Cambridge Bioscience). After the coating procedure, 0.2 mL of cells at a density of 1×10^6 cells/mL in phosphate-buffered saline (PBS) was collected, and 1 μL of 0.2 mM NucView 488 substrate stock solution and 2.5 μL of propidium iodide (PI) stock solution (BD Biosciences) were added. After the solutions had been mixed, the cells were incubated at 37 °C and 5% CO_2 for 15−30 min, protected from light. Before cell analysis on an ImageStream X Mark II Imaging Flow Cytometer (Amnis)—nearly 9500 events for each concentration—200 μL of PBS was added to each sample. Samples were analyzed using IDEAS software (Merck Millipore). The tetrazolium-based standard 3-(4,5-dimethylthiazol-2-yl)-2,5-diphenyltetrazolium bromide (MTT) (Sigma Life Science) assay was carried out to assess the cell metabolic activity in the presence of different PLL concentrations. Cells at a density of $\sim 1 \times 10^5$/mL were seeded in 24-well plates and incubated at 37 °C and 5% CO_2 for 4, 24, 72, and 168 h. Following the incubation period, supplemented DMEM was replaced by serum-free DMEM and MTT solution (5 mg/mL in PBS), reaching a final concentration of 0.5 mg/mL. After a 4-h incubation period at 37 °C and 5% CO_2, serum-free DMEM was replaced by 200 μL of isopropanol under gentle agitation for 20−30 min and protected from light. Afterward, 100 μL of dissolved formazan was transferred to a 96-well plate, and the absorbance was measured with a spectrophotometer (Sunrise, Tecan) at 570 nm. The Live/Dead (Molecular Probes by Life Technologies) assay was used to evaluate the cytotoxicity caused by different PLL concentrations. Reagent stock solutions were removed from the freezer and warmed to room temperature and were prepared using the manufacturer's recommendations to obtain a 4 μM ethidium homodimer (EthD-1) and 2 μM calcein AM solution. For microscope slides (immediately after coating imaging), approximately 5×10^4 cells were cultured in slides, 100 μL of Live/Dead working solution was added, and the cells were incubated for 40 min at room temperature. For six-well plates (24 h after coating process), approximately 2×10^5 cells were cultured in six-well plates, 500 μL of Live/Dead working solution was added, and the cells were incubated for 40 min at room temperature. Slides and well plates were imaged with a fluorescence microscope (Leica DM IL LED, Leica Microsystems) using the indicated filters: fluorescein filter for calcein (live cells) and Texas red filter for ethidium homodimer (dead cells). Images were captured using SPOT Advanced software (SPOT Imaging Solutions).

2.4. Cell Fixation and Probe Staining for Confocal Microscopy. Cells were fixed immediately after the coating process or 1 day later once attached and proliferating using 4% paraformaldehyde (Sigma Life Science) for 15 min at room temperature. Cells were washed three times using 0.1% DPBS/Tween 20 (Sigma Life Science) and phalloidin (1 mg/mL, Sigma Life Science) added during a 20-min light-protected incubation period at room temperature. After further washing, 4′,6-diamidino-2-phenylindole (DAPI; 1:2500 solution, Vector Laboratories) was added, and the solution was subjected to a 15-min light-protected incubation period at room temperature. Cells were washed and resuspended in 500 μL of NaCl solution (0.15 M). Fixed cells were stored protected from light at 4 °C. Cells coated with PLL-FITC were visualized using a Leica TCS SP2 UV AOBS MP (Upright) point scanning confocal microscope (Leica Microsystems) at 20× magnification.

2.5. Polymer Uptake Detection by Transmission Electron Microscopy. The polymer localization examination was performed using a Phillips CM 100 Compustage (FEI) transmission electron microscope (Philips), and digital images were collected using an AMT CCD camera (Deben). Coated cells were fixed using a solution of 2% glutaraldehyde (TAAB Laboratory Equipment) in sodium cacodylate buffer at 4 °C, followed by a secondary fixation with 1% osmium tetroxide (Agar Scientific). Cells were subjected to several dehydration steps, embedded in resin, and cut in ultrathin sections (approximately 70 nm) using a diamond knife on a Leica EM UC7 ultramicrotome (Leica Microsystems). The sections were stretched with chloroform to eliminate compression and mounted on Pioloform-filmed copper grids (Agar Scientific).

2.6. Polymer Metabolization by Flow-Activated Cell Sorting. PLL-FITC-coated cells were analyzed 15 min, 24 h, and 48 h following coating. A cell density of $\sim 2 \times 10^6$/mL in HBSS without phenol red was prepared, and data were acquired on a FACSCalibur flow cytometer (BD Biosciences). Forward-scattered and sideways-scattered data were used to gate in intact cells and exclude cell debris. The obtained data were analyzed using Flowing Software v2.5.

2.7. G-Band Karyotyping. Cells were incubated with 0 or 10 μg/mL PLL until 50−80% confluency. On the day before the harvest, 10 μL/mL colcemid was added to each cell culture flask and incubated overnight. Cells were gently washed with DPBS, and trypsin was used to detach the cells. After a 7-min 400*g* centrifugation, 0.075 M KCl was added to the pellet with vortexing to ensure mixing. Then, 5 mL of Fresh Carnoy's Fixative was added dropwise, and another 5 mL of the same fixative added without mixing. Subsequently, the mixture was centrifuged at 400*g*, the supernatant was removed, and an additional 5 mL of fixative was added. To evaluate whether the slide provided good-quality information on the harvest, the following protocol was used: Cells were centrifuged at 400*g* for 5 min, and the supernatant was removed until only 300 to 500 μL remained, after which the cells were gently resuspended. Drops of the cell suspension were pipetted onto a slide, and fresh Carnoy's Fixative was added. Finally, for G-banding, the slides were aged at 60 °C overnight and immersed in 50 mL of PBS and 1 mL of 10× trypsin (0.5%), before being stained with Leishmann and Giemsa Staining Solution for 3 min. Slides were then allowed to completely dry. DPX mountant was finally added, and the slides were observed using a light microscope at 1250× magnification.

2.8. Cell Aggregation Test and Aggregate Area Quantification. A quantity of 1×10^6 10 μg/mL coated cells were suspended in 1 mL of complete media inside a 1 mL syringe. Ten drops were dispensed through a 21-gauge needle every hour up to 3 h. The drops were observed using the fluorescence microscope stated above. Between depositions, cells were incubated at 37 °C and 5% CO_2. The images obtained were processed using ImageJ software (National Institutes of Health). Each image from the triplicate biological experiment was processed using the *Threshold* function, and 20 samples were selected at random through *ROI manager* and subjected to area measurement.

DOI: 10.1021/acsami.6b16434
ACS Appl. Mater. Interfaces 2017, 9, 12967−12974

2.9. Inkjet Cell Printing. A Jetlab 4 (Microfab Technologies, Inc.) single-orifice piezoelectric printer with an in-house reservoir was used. Two 1 × 10^6 cell/mL bioinks containing 10 μg/mL PLL-coated or noncoated cells were dispensed from a 60-μm-diameter inkjet printhead (MJ-AT-01−60−8MX, Microfab Technologies, Inc.) into a six-well plate. Ten depositions of 50 droplets each were printed in a 1 × 10 array at seven time points (from 0 to 60 min) in 10-min increments. Each sample was analyzed after deposition using an inverted microscope (Leica DM IL LED, Leica Microsystems), and the number of cells was recorded.

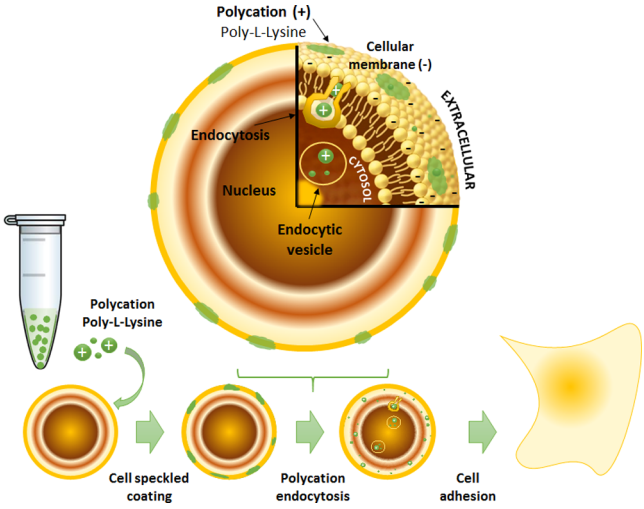

Figure 1. Illustration of temporary cellular speckled coating using poly(L-lysine) and further uptake of the biodegradable polycation.

2.10. Statistical Analysis. Data are expressed as mean ± standard deviation. Mean values and standard deviations were calculated from three independent experiments of triplicates per group. Comparisons were performed by one-way analysis of variance (ANOVA) in conjunction with Tukey's multiple comparison test using levels of statistical significance of $P < 0.05$ (*), $P < 0.01$ (**), $P < 0.001$ (***), and $P < 0.0001$ (****).

3. RESULTS AND DISCUSSION

Cells immersed in the polymeric solutions produced a polycationic coating that was speckled rather than a complete capsule (Figure 1), as a result of electrostatic attraction of PLL to the cell membrane, with the positively charged polymer attracted by the negatively charged membrane.[25]

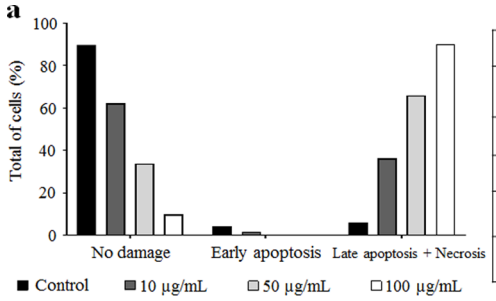

PI Positive		
[C] (μg/mL)	Only PI Positive (%)	Only PI and PI + NucView (%)
Control	5.13	5.88
10	35.38	36.18
50	31.20	65.92
100	24.86	90.05

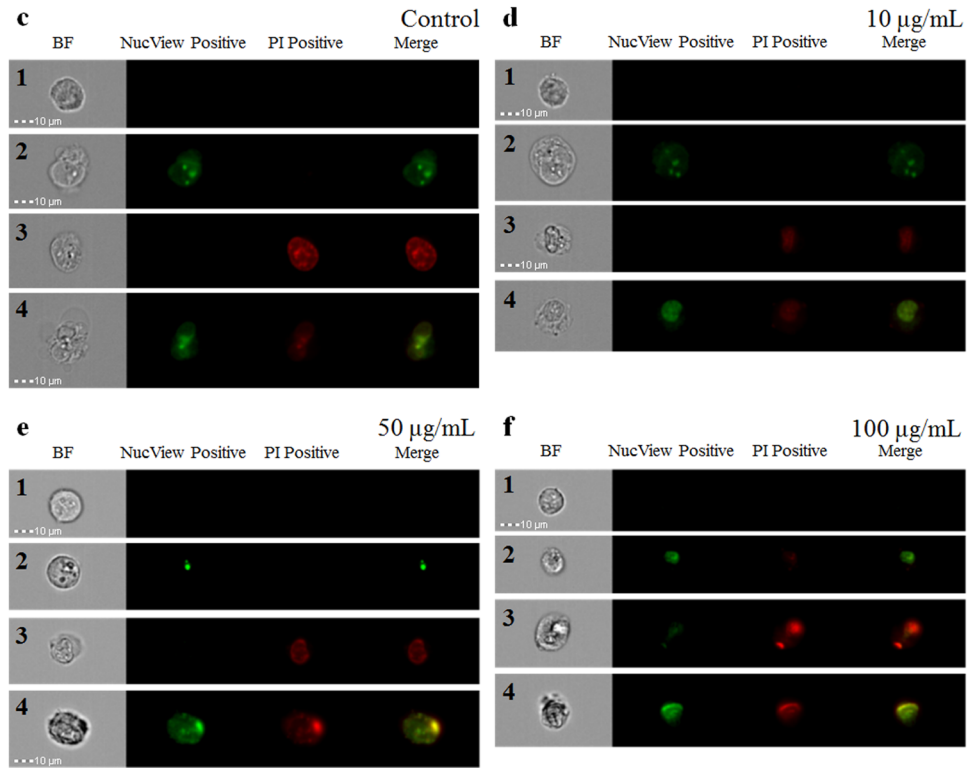

Figure 2. Caspase-3 activity and cell permeability detection for U2OS cells. (a) Cell death scores after analysis. (b) Total number of events for PI positive cells. (c−f) ISx analysis samples: (c) control, (d) 10 μg/mL, (e) 50 μg/mL, (f) 100 μg/mL. Scale bars, 10 μm. Double negative, apoptotic cells, necrotic cells, and double positive are represented by the numbers 1, 2, 3, and 4, respectively.

DOI: 10.1021/acsami.6b16434
ACS Appl. Mater. Interfaces 2017, 9, 12967−12974

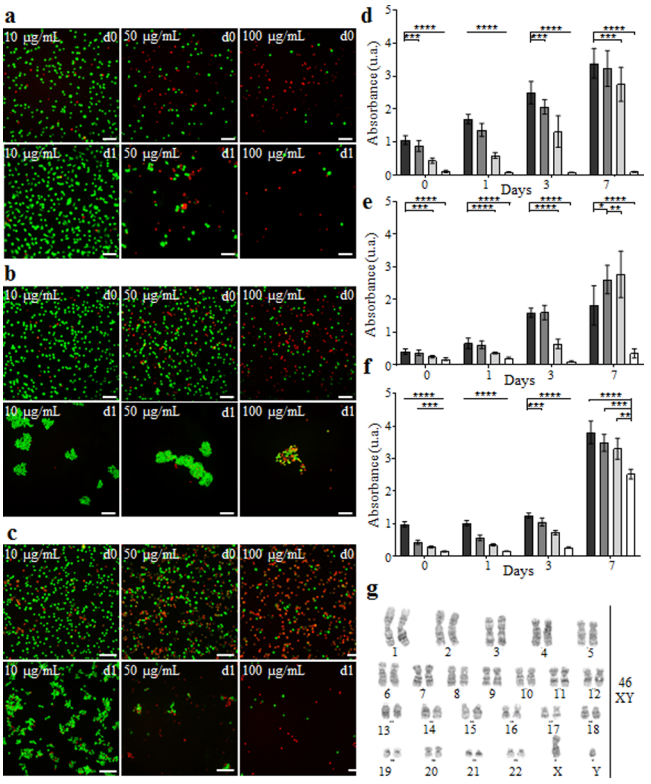

Figure 3. Survival indicators of coated (a,d) U2OS, (b,e) TC-71, and (c,f) Neo-NHDF cells: (a–c) Live/Dead assay at 4 h (d0) and day 1; (d–f) MTT assay scores for days 0, 1, 3, and 7. Dark gray bars represent untreated cells; gray, light gray, and white bars represent cells coated in 10, 50, and 100 μg/mL solution, respectively. The data are shown as mean ± SD. Results are relative to control at the same time point. *, **, ***, and **** indicate a significant difference between groups at the levels $p < 0.05$, $p < 0.01$, $p < 0.001$, and $p < 0.0001$, respectively. Error bars represent the standard deviation ($n = 3$). (g) 10 μg/mL coated Neo-NHDF cells obtained after speckled coating are karyotypically normal. Scale bars for Live/Dead images are 100 μm.

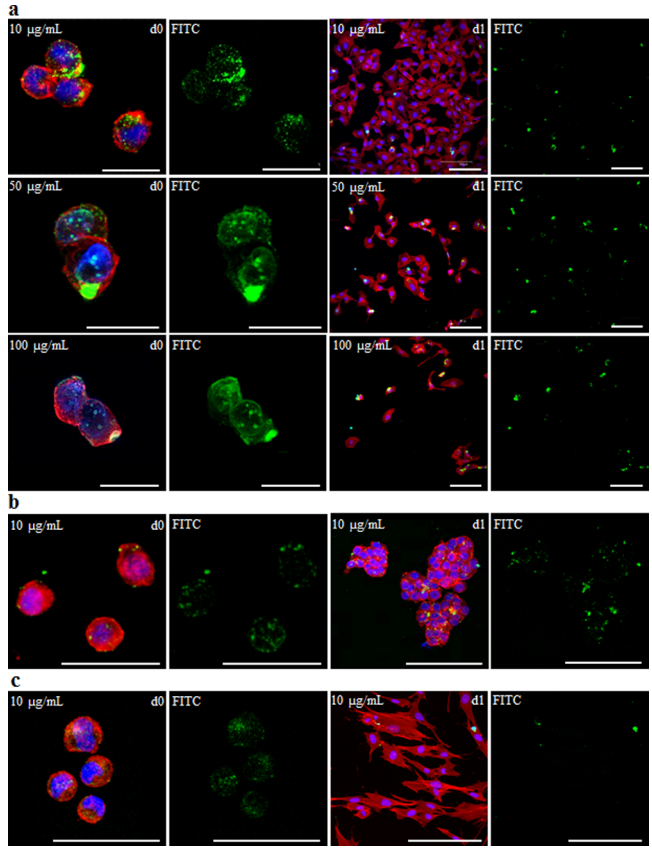

Figure 4. Cell and shell morphology after PLL speckled coating. U2OS, TC-71 and Neo-NHDF (a-c, respectively) show concentration-dependent capsule tightly fitting the cellular membrane immediately after coating (d0). Shell release through internalization processes and attachment and proliferation were observed 1 day after coating (d1). The nucleus is represented in blue (DAPI), f-actin in red (Phalloidin), and the PLL capsule in green (FITC). Scale bars, 50 μm (day 0) and 150 μm (day 1).

3.1. In Vitro Cell Viability Studies. Cell death as a result of the coating process was studied through caspase-3 activity and cell permeability detection on U2OS cells (Figure 2). It was observed (Figure 2a) that, immediately after encapsulation, only 62% of the 10 μg/mL coated cells presented a healthy morphology and were negative for both PI and NucView, compared to 90% for untreated cells. For the other two concentrations, 50 and 100 μg/mL, 34% and 10% of cells, respectively, were viable. For the dead cells, it was difficult to differentiate between late apoptosis and necrosis, perhaps as a result of caspase or other protease activity cleaving the probe in the dead cells. However, we consider necrosis as a result of the coating process to be the most likely cause of cell death, and the cell morphologies (Figure 2c–f) support this view. The nature of this damage is considered to be related to the change in permeability caused by polycation-induced membrane pores, as the majority of dead cells were PI-positive, which would be in agreement with past studies for a range of polycations.[10−14]

Figure 3 indicates that the cell behavior for those cells that survived the coating process was dependent on both the polymer concentration and the cell type. U2OS cells coated using the 10 μg/mL PLL solution (Figure 3a,d) revealed a metabolic activity similar to that of the untreated cells (control) during the course of the experiment. Coating with the 50 μg/mL PLL solution reduced cell metabolic activity by more than 50% at day 0 compared to the control; however, a recovery compared to the control was observed at later time points. Coating with the 100 μg/mL concentration showed a cytotoxic response. For the TC-71 cells (Figure 3b,e), the response was similar to that for the U2OS cells: Cells coated using the 10 μg/mL concentration exhibited a metabolic behavior identical to that of the control; the 50 μg/mL concentration initially decreased cell metabolic activity with a recovery between days 3 and 7; and a cytotoxic response was observed for the 100 μg/mL concentration, although a slightly slower cytotoxic response was found than for the U2OS cells at the end of the experiment. The clustering of the TC-71 cells (Figure 3b) is normal proliferative behavior for this cell type. The Neo-NHDF (Figure 3c,f) cell behavior was slightly different. These cells presented an initially lower metabolic activity compared to control for the 10 μg/mL concentration, although the activity recovered steadily over the first 3 days postcoating. The 50 μg/mL coated cells exhibited similar behavior in terms of metabolic activity, but from a lower starting point and with a marked recovery at days 3 and 7. The 100 μg/mL coated cells barely presented any metabolic activity at day 0, recovered slowly up to day 3, and then showed a significant recovery between days 3 and 7.

For all three cell types, the higher concentrations of PLL solution, namely, 50 and 100 μg/mL, were found to cause

DOI: 10.1021/acsami.6b16434
ACS Appl. Mater. Interfaces 2017, 9, 12967−12974

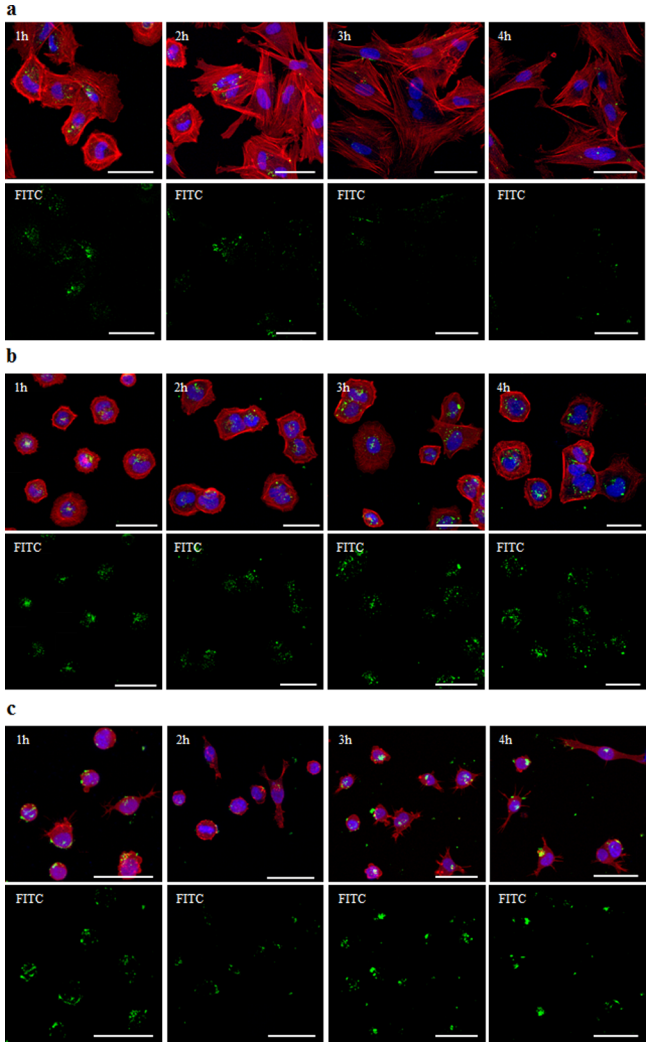

Figure 5. PLL internalization and metabolization in the first 4 h after coating with 10 μg/mL concentration allows normal cell attachment and proliferation. (a) Neo-NHDF cells attached within 1 h and metabolized almost all polymer within 4 h. (b) Osteosarcoma cells attached within 1 h, but slow polycation metabolization was observed in the firsts 4 h. (c) TC-71 cells started attaching soon after the coating procedure, but polymer metabolization was again slow. Staining similar to that in Figure 4. Scale bars (same for all images), 50 μm.

lower levels of metabolic activity in cells than the 10 μg/mL solution coated cells. However, 1 week postcoating, cells coated using the 50 μg/mL solution were as metabolically active as the control and 10 μg/mL coated cells. The 100 μg/mL concentration proved to be toxic for both cancer cell lines, but was better tolerated by the Neo-NHDF cells. TC-71 and Neo-NHDF 10 μg/mL coated cells were karyotypically unchanged after being coated (Figure 3g and Figure S1).

3.2. Cell and Coating Morphologies. Analysis of the cell and speckled coating morphologies showed cell integrity after the process (Figure 4) and indicated that the polycation was tightly bound to the membrane for all three cell types. However, the completeness of the coating was dependent on polymer availability, taking the form of a closed envelope only at higher concentrations (Figure 4a and Figure S2). Cells coated with the 10 μg/mL PLL solution had surfaces speckled with PLL particles (Figure 4a–c). One day after coating, the cells had ingested the PLL and exhibited normal attachment

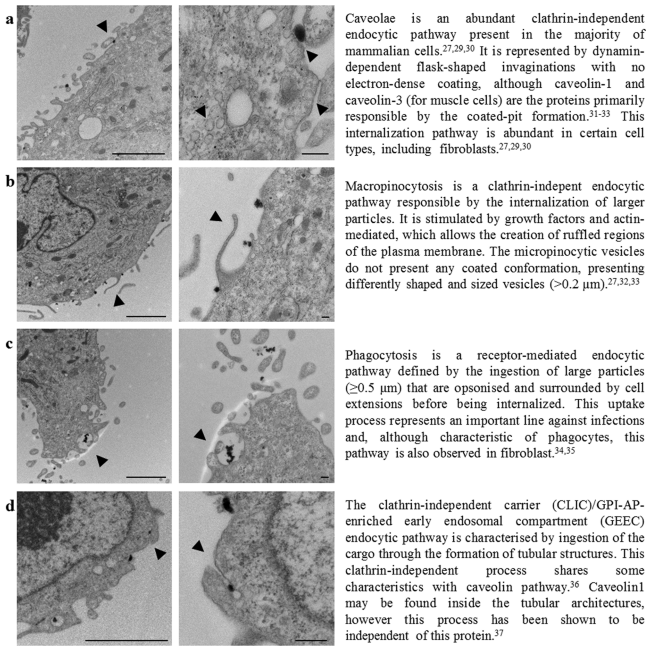

Figure 6. PLL is actively internalized by coated cells using size-dependent endocytic pathways.[27,29−37] (a−c) Three different endocytic pathways were observed for human fibroblasts once fixed immediately after speckled coating: caveolar-type endocytosis, micropinocytosis, and phagocytosis. (d) CLIC/GEEC-type endocytosis noted on osteosarcoma cells. All micrographs represent day 0 cells coated using a 10 μg/mL PLL solution. Scale bars are 2 μm and 200 nm for the left and right columns, respectively.

and proliferation: U2OS cells presented a heterogeneous population showing attachment and spreading, TC-71 cells grew in clumps, and fibroblasts were flattened and elongated. Additionally, signs of increasing polymer ingestion and metabolization by healthy cells could be observed at day one.

3.3. Polymer Uptake and Metabolization. Cells coated using the 10 μg/mL PLL concentration were able to attach within 1 h, after which the polymer was rapidly internalized (Figure 5). The different cell types showed different PLL metabolization rates, with the fibroblasts metabolizing the majority of the polymer in the first 4 h postcoating, with little PLL evident at this time point (Figure 5a), and the U2OS and TC-71 cell lines metabolizing the polymer at lower rates, with PLL still evident (Figure 5b,c).

To confirm polycation uptake and metabolization, samples were analyzed by transmission electron microscopy. A range of endocytic pathways were observed by transmission electron microscopy (Figure 6); however, specific-pathway inhibitors must be used to clearly identify each pathway and its dependency on the size of the micro- or nanoparticles being ingested, as observed in previous studies.[26−28] The higher PLL concentrations damaged the cell membrane through uncontrolled polymer internalization, leading to cell death by necrosis (Figure S3).

The metabolization rate was quantified for the cells coated using the 10 μg/mL PLL solution using FACS (Figure 7). PLL-FITC-coated cells showed a marked increase in fluorescence intensity when compared to the control population, decreasing progressively over the two-day period as the cells ingested and metabolized the polymer and approaching the control values after 2 days. Over this longer time period, the rates at which the fibroblasts and TC-71 cells metabolized the polymer were qualitatively higher than that for the U2OS cells, as indicated by

DOI: 10.1021/acsami.6b16434
ACS Appl. Mater. Interfaces 2017, 9, 12967−12974

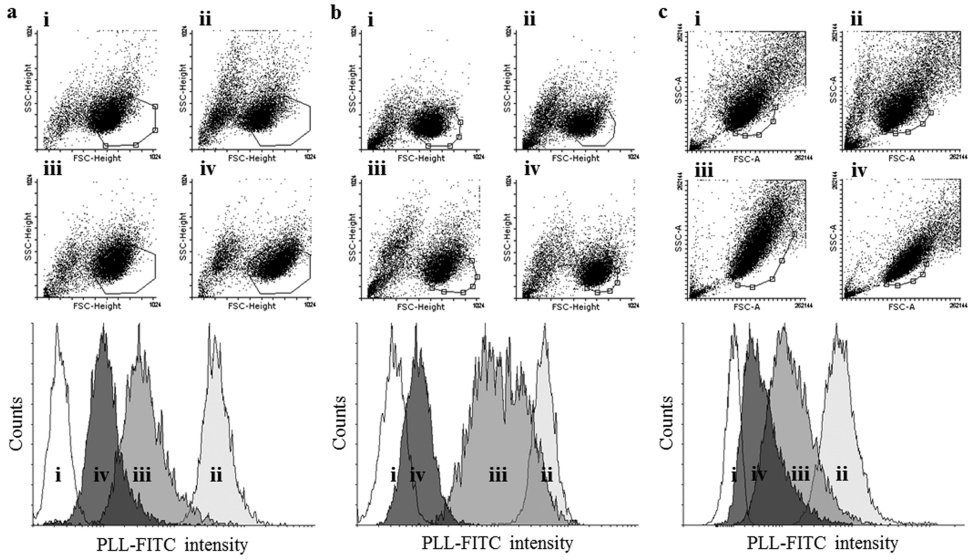

Figure 7. FACS gating and histograms for live (A) U2OS, (B) TC-71, and (C) Neo-NHDF cells coated using a 10 μg/mL PLL solution. i is control (day 0), and ii, iii, and iv represent days 0, 1, and 2, respectively.

the relative overlaps between the control populations and the day 2 populations.

3.4. Polycation Coating for the Avoidance of Cell Agglomeration and Its Use in Cell Printing. Using a syringe, coated and noncoated cells were dispensed onto glass slides and observed under a microscope (Figure 8a,b), and the areas of aggregates were quantified (Figure 8c). Aggregate area was higher at time zero for untreated cells and increased at a much higher rate than for the treated cells. After 3 h of cell incubation inside the syringe, 10 μg/mL coated cells were largely free of natural cell agglomeration, remaining dispersed with a minimum formation of small aggregates (Figure 8a). Noncoated cells started to agglomerate after 2 h, with sizable cell clusters observed after 3 h (Figure 8b).

The reliability of bioprocessing techniques, such as inkjet cell printing, is compromised by cell aggregation issues. It was observed that noncoated cells did not reliably print and aggregated and blocked the printer nozzle between 10 and 20 min after the start of printing. In contrast, 10 μg/mL coated cells allowed repeatable printing with about 1 cell per drop over the course of a 60-min printing session without cell clogging, indicating that the polycationic coating had effectively stabilized the bioink.

4. CONCLUSIONS

In this study, we developed an efficient and temporary single-cell PLL coating process. This process allows for the development of a high-efficiency and tightly fitting speckled coating. The coating process causes necrosis when high concentrations of PLL are used, but 70% cell viability relative to the control is possible when a concentration of 10 μg/mL is used. Cells can ingest, through multiple endocytic pathways, and metabolize the polymer, returning to phenotypically normal cell behavior shortly after ingestion. It was demonstrated that the coating with the lowest PLL concentration effectively inhibited the creation of oversized cell agglomerates, and preliminary studies showed that bioink stabilization for inkjet cell printing is one possible use of this temporary polycationic coating. In conclusion, these findings support the development of single-cell coating by polycationic coating as a potential method to be applied in cell processing to temporarily prevent the formation of cellular aggregates.

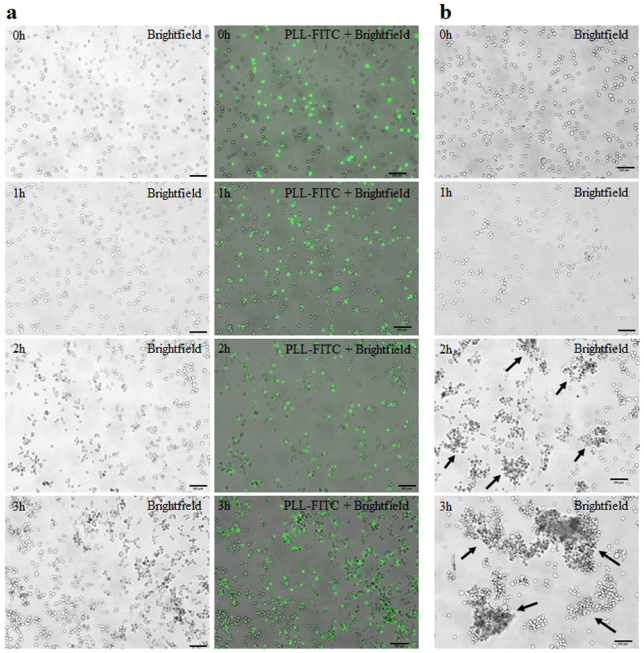

Cell aggregation area (μm²)		
Time(h)	Control	10 μg/mL
0	335.09±169.79	162.79±106.21
1	1151.38±1164.86	321.56±153.26
2	2261.96±1677.491	547.96±448.56
3	11036.56±12552.41	1177.60±789.19

Figure 8. Speckled coating avoids cell aggregation and allows repeatable printing results. (a) U2OS cells speckle-coated with a 10 μg/mL coating present dispersion when deposited through a 21 G needle at different times after the coating procedure. (b) Uncoated U2OS cells present high degree of agglomeration (arrows) within the deposition times. Scale bars, 100 μm. (c) Development of cell aggregates over time. (d) Inkjet bioprinting of control and 10 μg/mL PLL speckle-coated U2OS cells.

DOI: 10.1021/acsami.6b16434
ACS Appl. Mater. Interfaces 2017, 9, 12967−12974

■ ASSOCIATED CONTENT

Supporting Information

The Supporting Information is available free of charge on the ACS Publications website at DOI: 10.1021/acsami.6b16434.

Karyotype after coating; confocal microscopy, TEM images, and cell aggregation quantification (PDF)

Data supporting this publication is openly available under an 'Open Data Commons Open Database License'. Additional metadata are available at: http://dx.doi.org/10.17634/122951-2. Please contact Newcastle Research Data Service at rdm@ncl.ac.uk for access instructions.

■ AUTHOR INFORMATION

Corresponding Author

*E-mail: Ana.Ferreira-Duarte@newcastle.ac.uk.

ORCID

Ricardo D. C. Ribeiro: 0000-0003-1591-0499

Ana M. Ferreira: 0000-0002-7728-1619

Author Contributions

A.M.F., M.B., and K.D. conceived the study; all authors contributed to the design of the study; R.R, D.P., D.J., and M.B. performed the experiments and acquired the data. All authors analyzed the data and contributed to drafting and reviewing the manuscript.

Notes

The authors declare no competing financial interest.

■ ACKNOWLEDGMENTS

The work reported in this article was partially funded by the Arthritis Research UK Tissue Engineering Centre (19429) and the EPSRC Centre for Innovative Manufacture in Medical Devices (MeDe Innovation; EP/K029592). R.D.C.R. acknowledges support from Newcastle University for his Ph.D. studentship. D.P. was supported by a JGW Patterson Foundation Fellowship and an NC3Rs Training Fellowship. The authors also thank T. Booth for the confocal microscopy image acquisition at the Bioimaging Unit (Newcastle University, U.K.), K. White for help in interpretation of the TEM images at the Electron Microscopy Research Services (Newcastle University, U.K.), and G. Cuthbert for karyotype analyses at the Institute of Genetic Medicine (Newcastle University, U.K.).

■ ABBREVIATIONS

PLL, poly(L-lysine)

■ REFERENCES

(1) Wang, S.; Guo, Z. Bio-inspired Encapsulation and Functionalization of Living Cells with Artificial Shells. *Colloids Surf., B* **2014**, *113*, 483−500.

(2) Faulkner-Jones, A.; Greenhough, S.; King, J. A.; Gardner, J.; Courtney, A.; Shu, W. Development of a Valve-based Cell Printer for the Formation of Human Embryonic Stem Cell Spheroid Aggregates. *Biofabrication* **2013**, *5*, 015013.

(3) Murphy, S.; Atala, A. 3D Bioprinting of Tissues and Organs. *Nat. Biotechnol.* **2014**, *32*, 773−785.

(4) Kellam, B.; De Bank, P. A.; Shakesheff, K. M. Chemical Modification of Mammalian Cell Surfaces. *Chem. Soc. Rev.* **2003**, *32*, 327−337.

(5) Wilson, J. T.; Krishnamurthy, V. R.; Cui, W.; Qu, Z.; Chaikof, E. L. Noncovalent Cell Surface Engineering with Cationic Graft Copolymers. *J. Am. Chem. Soc.* **2009**, *131*, 18228.

(6) Prescher, J. A.; Bertozzi, C. R. Chemistry in Living Systems. *Nat. Chem. Biol.* **2005**, *1*, 13−21.

(7) Rabuka, D.; Forstner, M. B.; Groves, J. T.; Bertozzi, C. R. Noncovalent Cell Surface Engineering: Incorporation of Bioactive Synthetic Glycopolymers into Cellular Membranes. *J. Am. Chem. Soc.* **2008**, *130*, 5947−53.

(8) Decher, G. Fuzzy Nanoassemblies: Toward Layered Polymeric Multicomposites. *Science* **1997**, *277*, 1232−1237.

(9) Fakhrullin, R. F.; Zamaleeva, A. L.; Minullina, R. T.; Konnova, S. A.; Paunov, V. N. Cyborg Cells: Functionalization of Living Cells with Polymers and Nanomaterials. *Chem. Soc. Rev.* **2012**, *41*, 4189−4206.

(10) Fischer, D.; Li, Y.; Ahlemeyer, B.; Krieglstein, J.; Kissel, T. In Vitro Cytotoxicity Testing of Polycations: Influence of Polymer Structure on Cell Viability and Hemolysis. *Biomaterials* **2003**, *24*, 1121−1131.

(11) Menger, F.; Seredyuk, V. A.; Kitaeva, M. V.; Yaroslavov, A. A.; Melik-Nubarov, N. S. Migration of Poly-L-lysine through a Lipid Bilayer. *J. Am. Chem. Soc.* **2003**, *125*, 2846−2847.

(12) Bieber, T.; Meissner, W.; Kostin, S.; Niemann, A.; Elsasser, H. P. Intracellular Route and Transcriptional Competence of Polyethylenimine-DNA Complexes. *J. Controlled Release* **2002**, *82*, 441−454.

(13) Hong, S.; Leroueil, P. R.; Janus, E. K.; Peters, J. L.; Kober, M. M.; Islam, M. T.; Orr, B. G.; Baker, J. R., Jr; Banaszak Holl, M. M. Interaction of Polycationic Polymers with Supported Lipid Bilayers and Cells: Nanoscale Hole Formation and Enhanced Membrane Permeability. *Bioconjugate Chem.* **2006**, *17*, 728−734.

(14) Vaidyanathan, S.; Anderson, K. B.; Merzel, R. L.; Jacobovitz, B.; Kaushik, M. P.; Kelly, C. N.; van Dongen, M. A.; Dougherty, C. A.; Orr, B. G.; Banaszak Holl, M. M. Quantitative Measurement of Cationic Polymer Vector and Polymer-pDNA Polyplex Intercalation into the Cell Plasma Membrane. *ACS Nano* **2015**, *9*, 6097−6109.

(15) Matsusaki, M.; Akashi, M. Control of Extracellular Microenvironments Using Polymer/Protein Nanofilms for the Development of Three-dimensional Human Tissue Chips. *Polym. J. (Tokyo, Jpn.)* **2014**, *46*, 524−536.

(16) Johnston, A.; Cortez, C.; Angelatos, A.; Caruso, F. Layer-by-Layer Engineered Capsules and their Applications. *Curr. Opin. Colloid Interface Sci.* **2006**, *11*, 203−209.

(17) Ai, H.; Jones, S.; Lvov, Y. Biomedical Applications of Electrostatic Layer-by-layer Nano-assembly of Polymers, Enzymes, and Nanoparticles. *Cell Biochem. Biophys.* **2003**, *39*, 23−43.

(18) Caruso, F.; Trau, D.; Mohwald, H.; Renneberg, R. Enzyme Encapsulation in Layer-by-Layer Engineered Polymer Multilayer Capsules. *Langmuir* **2000**, *16*, 1485−1488.

(19) Silva, J.; Reis, R.; Mano, J. Biomimetic Extracellular Environment Based on Natural Origin Polyelectrolyte Multilayers. *Small* **2016**, *12*, 4308−4342.

(20) Dubas, S.; Schlenoff, J. Factors Controlling the Growth of Polyelectrolyte Multilayers. *Macromolecules* **1999**, *32*, 8153−8160.

(21) Li, W.; Guan, T.; Zhang, X.; Wang, Z.; Wang, M.; Zhong, W.; Feng, H.; Xing, M.; Kong, J. The Effect of Layer-by-Layer Assembly Coating on the Proliferation and Differentiation of Neural Stem Cells. *ACS Appl. Mater. Interfaces* **2015**, *7*, 3018−3029.

(22) Balkundi, S. S.; Veerabadran, N. G.; Eby, D. M.; Johnson, G. R.; Lvov, Y. M. Encapsulation of Bacterial Spores in Nanoorganized Polyelectrolyte Shells. *Langmuir* **2009**, *25*, 14011−14016.

(23) Diaspro, A.; Silvano, D.; Krol, S.; Cavalleri, O.; Gliozzi, A. Single Living Cell Encapsulation in Nano-organized Polyelectrolyte Shells. *Langmuir* **2002**, *18*, 5047−5050.

(24) Vormoor, B.; Knizia, H. K.; Batey, B. A.; Almeida, G. S.; Wilson, I.; Dildey, P.; Sharma, A.; Blair, H.; Hide, I. G.; Heidenreich, O.; Vormoor, J.; Maxwell, R. J.; Bacon, C. M. Development of a Preclinical Orthotopic Xenograft Model of Ewing Sarcoma and Other Human Malignant Bone Disease Using Advanced In Vivo Imaging. *PLoS One* **2014**, *9*, e85128.

(25) Wilson, J. T.; Chaikof, E. L. Molecular Engineering of Cell and Tissue Surfaces with Polymer Thin Films. In *Micro- and Nanoengineering of the Cell Surface*; Karp, J. M., Zhao, W., Eds.; Elsevier: Oxford, U.K., 2012; Chapter 13, pp 281−314.

(26) Kumari, S.; Mg, S.; Mayor, S. Endocytosis Unplugged: Multiple Ways to Enter the Cell. *Cell Res.* **2010**, *20*, 256−275.
(27) Kastl, L.; Sasse, D.; Wulf, V.; Hartmann, R.; Mircheski, J.; Ranke, C.; Carregal-Romero, S.; Martínez-López, J. A.; Fernández-Chacón, R.; Parak, W. J.; Elsasser, H.-P.; Rivera-Gil, P. Multiple Internalization Pathways of Polyelectrolyte Multilayer Capsules into Mammalian Cells. *ACS Nano* **2013**, *7*, 6605−6618.
(28) Doherty, G.; McMahon, H. Mechanisms of Endocytosis. *Annu. Rev. Biochem.* **2009**, *78*, 857−902.
(29) Piccinotti, S.; Kirchhausen, T.; Whelan, S. Uptake of Rabies Virus into Epithelial Cells by Clathrin-mediated Endocytosis Depends upon Actin. *J. Virol.* **2013**, *87*, 11637−11647.
(30) Kirkham, M.; Parton, R. Clathrin-independent Endocytosis: New Insights into Caveolae and Non-caveolar Lipid Raft Carriers. *Biochim. Biophys. Acta, Mol. Cell Res.* **2005**, *1745*, 273−286.
(31) Parton, R. G.; Simons, K. The Multiple Faces of Caveolae. *Nat. Rev. Mol. Cell Biol.* **2007**, *8*, 185−194.
(32) Pelkmans, L.; Helenius, A. Endocytosis Via Caveolae. *Traffic* **2002**, *3*, 311−320.
(33) Lim, J.; Gleeson, P. Macropinocytosis: An Endocytic Pathway for Internalising Large Gulps. *Immunol. Cell Biol.* **2011**, *89*, 836−843.
(34) Mercer, J.; Helenius, A. Virus Entry by Macropinocytosis. *Nat. Cell Biol.* **2009**, *11*, 510−520.
(35) Flannagan, R.; Jaumouille, V.; Grinstein, S. The Cell Biology of Phagocytosis. *Annu. Rev. Pathol.: Mech. Dis.* **2012**, *7*, 61−98.
(36) Chaudhary, N.; Gomez, G. A.; Howes, M. T.; Lo, H. P.; McMahon, K. A.; Rae, J. A.; Schieber, N. L.; Hill, M. M.; Gaus, K.; Yap, A. S.; Parton, R. G. Endocytic Crosstalk: Cavins, Caveolins, and Caveolae Regulate Clathrin-independent Endocytosis. *PLoS Biol.* **2014**, *12*, e1001832.
(37) McMahon, H. T.; Boucrot, E. Molecular Mechanism and Physiological Functions of Clathrin-Mediated Endocytosis. *Nat. Rev. Mol. Cell Biol.* **2011**, *12*, 517−533.

DOI: 10.1021/acsami.6b16434
ACS Appl. Mater. Interfaces 2017, 9, 12967−12974